Journal of Colloid and Interface Science **229,** 107–117 (2000)
doi:10.1006/jcis.2000.6956, available online at http://www.idealibrary.com on IDEAL®

Rheological and Electrokinetic Properties of Sodium Montmorillonite Suspensions

I. Rheological Properties and Interparticle Energy of Interaction

J. D. G. Durán, M. M. Ramos-Tejada, F. J. Arroyo,[1] and F. González-Caballero

Departamento de Física Aplicada, Facultad de Ciencias, Universidad de Granada, 18071 Granada, Spain

Received November 9, 1999; accepted May 8, 2000

In this article, we describe the rheology of Na montmorillonite suspensions as a function of pH, at constant ionic strength. The observed behavior is discussed quantitatively in terms of the potential energy of interaction between particles, keeping in mind the anisotropic nature of clay particles. The extended DLVO model that includes electrostatic, van der Waals, and polar acid–base contributions to the total energy is used. It is found that face-to-face interactions are virtually independent of pH, whereas edge-to-edge interactions are most attractive at the isoelectric point of edges (pH $\sim$ 7). The most significant variations occur in face-to-edge potential energy, with strong attractions at pH $<$ 7. Steady-state viscometry showed that the yield stress decreases up to an order of magnitude between pH 3 and pH 7, with a much slower rate of decrease in the 7–11 pH interval. Concerning oscillatory measurements, it is found that both the elastic (G') and viscous (G'') moduli are practically independent of frequency. It is also demonstrated that $G' > G''$, the difference being larger at acid pH values. These results, in addition to potential energy calculations, suggest the existence of an elastic, coagulated structure up to pH 7, whereas as the pH is increased such structure is more relaxed because of electrostatic repulsions. Similar conclusions are reached when creep–recovery data are analyzed.

Key Words: **sodium montmorillonite suspensions; zeta potential, surface free energy; DLVO theory; viscosity; suspension rheology; yield stress; viscoelastic behavior.**

INTRODUCTION

From[1] both the fundamental and applied points of view, there is a growing interest in the characterization of the properties of concentrated suspensions, probably the most interesting disperse systems in the industrial field. However, the knowledge of the internal structure of such suspensions and of the electric double layer surrounding each particle is not an easy task, the more so if the colloidal units are not homogeneous in size and shape. This happens to be the case with the clay suspensions studied in this work. The consequences that could derive from this kind of basic studies in very different areas of technology are evident and range from oil drilling fluids to the control of contaminant adsorption and transport in soils and natural waters (1–10).

Although interpretation of their results is not always easy, two techniques are most useful for the characterization of concentrated suspensions. These are rheological and dielectric measurements. They can provide (particularly if used jointly) information about both the internal structure and the particle interaction, as well as about the electrical properties, of the solid/liquid interface. In this part of the series, the rheological behavior of sodium montmorillonite suspensions is investigated and correlated with calculations of the interaction energy between the particles. The second part in this series is devoted to low-frequency dielectric dispersion measurements in the same suspensions.

The basic idea of this contribution is that the rheology of the suspensions can be quantitatively related to electric and thermodynamic properties of the interface and, in a more qualitative way, to their dielectric behavior. Few works have been published, to our knowledge, on the correlation between the response of colloidal systems to an oscillating mechanical shear (oscillatory rheometry) and to an alternating electric field (dielectric dispersions), despite its potential applications (2), that have been checked in the pharmaceutical research.

On the other hand, a much more thorough investigation has been reported on the explanation of the rheological properties of disperse systems on the basis of the analysis of interparticle interactions (9, 11–14), in the light of the classical DLVO theory. Here we intend to further study the relations existing between the rheology of clay systems (consisting of laminar, polydisperse particles) and the face-to-face, face-to-edge, and edge-to-edge interactions for different pH's, taking into account not only the electrostatic and van der Waals contributions but also the so-called hydration forces (15, 16) in the frame of the extended DLVO theory of suspension stability. In the accompanying paper (17), we analyze to what extent these features appear in the dielectric behavior of the suspensions.

[1] To whom correspondence should be addressed. Fax: 34-958-253498. E-mail: generi6@ugr.es.

0021-9797/00 $35.00

ESTIMATION OF THE INTERACTION ENERGY BETWEEN CLAY PARTICLES IN AQUEOUS MEDIA

A fundamental contribution to the energy of interaction between colloidal particles in suspension is electrostatic. Sodium montmorillonite (NaMt) particles are laminar in shape and their surface charge is not homogeneously distributed: face surfaces bear a negative charge generated by substitution of lattice ions and hence essentially independent of the composition of the aqueous medium, and edge surfaces have a pH-dependent charge. We consider both types of surfaces as flat plates (phase 1 is the face surfaces, phase 2 corresponds to the edges, and phase 3 is the dispersion medium). The interaction energy per unit area is calculated using the HHF model (18), based on the assumption of constant, moderate surface potentials (ψ_{01}, and ψ_{02}) and is more appropriate for surface-to-surface distances H larger than ~10 nm (9):

$$V_{i3j} = \frac{\varepsilon\kappa}{8\pi}\left[\left(\psi_{0i}^2 + \psi_{0j}^2\right)(1 - \coth\kappa H) + 2\psi_{0i}\psi_{0j}\,\mathrm{cosech}\,\kappa H\right]. \quad [1]$$

Above, ε is the dielectric constant of the medium, κ is the reciprocal Debye length, and subscripts (i, j) equal (1, 1), (1, 2), and (2, 2) for face-to-face, edge-to-face, and edge-to-edge interactions, respectively. The best approximation to either ψ_{0i} or ψ_{0j} in Eq. [1] is the diffuse-layer potential, but, since it is usually unknown, the zeta potential, ζ, is a reasonable alternative for not very highly charged surfaces.

The Lifshitz–van der Waals contribution to the potential energy can be obtained, for two large parallel plates separated by a distance H, from the equation (19)

$$V_{i3j}^{\mathrm{LW}} = -\frac{A_{i3j}}{12\pi H^2}, \quad i, j = 1, 2, \quad [2]$$

where A_{i3j} is the Hamaker constant corresponding to van der Waals interaction between phases i and j in the liquid medium 3. Interestingly, this constant can be determined if the LW component of the surface free energy of each phase, γ_k^{LW} ($k = 1, 2, 3$) is known (16).

$$A_{i3j} = -24\pi H_0^2\left[\left(\gamma_i^{\mathrm{LW}}\gamma_3^{\mathrm{LW}}\right)^{\frac{1}{2}} + \left(\gamma_j^{\mathrm{LW}}\gamma_3^{\mathrm{LW}}\right)^{\frac{1}{2}} - \left(\gamma_i^{\mathrm{LW}}\gamma_j^{\mathrm{LW}}\right)^{\frac{1}{2}} - \gamma_3^{\mathrm{LW}}\right], \quad [3]$$

where H_0 is the minimum separation distance (for $H < H_0$, strong Born repulsion would appear). The best approximation to H_0 is 1.58 Å (20) for very different systems.

As mentioned above, γ_k^{LW} is the Lifshitz–van der Waals component of the surface free energy or surface tension, γ_k, of phase k. Following the thermodynamic approach of Van Oss (16), γ_k consists of two additive contributions, related, respectively, to van der Waals and electron–acceptor/electron–donor (or acid/base in Lewis sense)

$$\gamma_k = \gamma_k^{\mathrm{LW}} + \gamma_k^{\mathrm{AB}}, \quad [4]$$

the latter being the result of the electron–donor (γ_k^-) and electron–acceptor (γ_k^+) characters of the material:

$$\gamma_k^{\mathrm{AB}} = 2\sqrt{\gamma_k^+\gamma_k^-}. \quad [5]$$

The acid/base component of the surface free energy gives rise in turn to another source of interaction between the particles, V_{i3j}^{AB}, sometimes known as structural or hydration forces. When the surfaces involved are hydrophilic (as it happens to be the case with clays), a repulsive short-range interaction results that depends exponentially on the distance H,

$$V_{i3j}^{\mathrm{AB}} = V_{i3j}^{\mathrm{AB}}(H_0)\,\exp\left[\frac{H_0 - H}{\lambda}\right], \quad [6]$$

where λ is the correlation length of water molecules, a good estimation of which is 1 nm for hydrophilic surfaces (16). The preexponential factor in Eq. [6] can also be calculated from the electron–donor and electron–acceptor components of the surface free energy of the phases involved (16):

$$V_{i3j}^{\mathrm{AB}}(H_0) = 2\left[\sqrt{\gamma_3^+}\left(\sqrt{\gamma_i^-} + \sqrt{\gamma_j^-} - \sqrt{\gamma_3^-}\right) + \sqrt{\gamma_3^-}\left(\sqrt{\gamma_i^+} + \sqrt{\gamma_j^+} - \sqrt{\gamma_3^+}\right) - \sqrt{\gamma_i^+\gamma_j^-} - \sqrt{\gamma_i^-\gamma_j^+}\right]. \quad [7]$$

EXPERIMENTAL

Materials

Since the starting material is a natural bentonite (from Almería, Spain) it bears a variety of exchangeable cations compensating the structural negative charge of the crystal lattice. In order to make surface studies in clay minerals as reproducible and repeatable as possible (whatever the sample origin), the first step was homoionization of the particles, i.e., the substitution of all exchangeable cations by only one species, Na^+ in our case. The homoionization procedure included stirring 50 g powder of the clay fraction $<2\ \mu$m with 250 ml of a 1 M NaCl solution for 1 h. The solids were separated from the solution by centrifugation and redispersed in the latter; this was repeated five times, and then the particles were repeatedly centrifuged and redispersed in Milli-Q water (Milli-Q Academic, Millipore, France) until the conductivity of the supernatant was bellow 10 μS/cm. Finally, the particles were dried at 100°C and stored in polyethylene containers. The specific surface area of dry NaMt was measured by means of N_2 adsorption using the BET multipoint method in a Quantasorb Jr (Quantachrome, USA). The value obtained, 54.1 m^2/g, is very similar to that reported by different authors (21, 22).

A bulk chemical analysis of the clay was performed by X-ray fluorescence. The results are displayed in Table 1, together with

TABLE 1
Bulk Chemical Composition Percentage of Original Bentonite (Taken from Ref. 4) and Sodium Montmorillonite (NaMt) Obtained by X-Ray Fluorescence Analysis

Compound	SiO_2	Al_2O_3	MgO	Fe_2O_3	Na_2O	K_2O	TiO_2	MnO_2	CaO	P_2O_5	H_2O	Other
Bentonite	58.52	20.19	6.70	2.70	1.35	0.61	—	—	1.08	—	8.98	—
NaMt	61.715	19.549	5.439	2.995	3.265	0.279	0.178	0.047	0.033	0.009	—	5.8

those reported in (4) for the original, untreated bentonite. Also, a Perkin–Elmer (USA) instrument was used to obtain the surface composition by XPS. The following elements and percentage abundances were detected: O (61.92%), Si (20.42%), Al (7.76%), C (5.14%), Na (2.37%), Mg (1.91%), and Fe (0.48%). Both types of analyses demonstrate that the homoionization was rather effective, since Na^+ is the only exchangeable cation detected in significant amount on the surface. Other exchangeable ions such as K^+ or Ca^{2+} were totally absent and only showed up (in small amounts) in the bulk analysis.

Analytical quality SiO_2 and Al_2O_3 powders were supplied by Riedel de Haën (Germany), and all other chemicals were also high purity from Panreac (Spain).

Electrophoretic Mobility

Electrophoretic mobility measurements were performed in a Malvern Zetasizer 2000 at $25.0 \pm 0.5^\circ$C. Given the polydispersity of the size and shape of the powders measured, the zeta potentials were estimated in all cases by means of the simple Helmholtz–Smoluchowski equation (21). All suspensions were prepared in 10^{-2} M NaCl solutions with variable pH's ranging between 3 and 11.

Surface Free Energy

The technique used to gain information about the surface free energy of NaMt was advancing contact angle measurement (23), using a Ramé-Hart 100-07-00 (USA) goniometer. The contact angles, θ, of three probe liquids of known γ^{LW}, γ^+, and γ^- (diiodomethane, ethylene glycol, and water; see Ref. 16) were measured. The clay solid surface was prepared by drying a concentrated (4% w/v) NaMt suspension uniformly spread on a dry, clean microscope glass slide. The powder was previously dispersed in a 10^{-2} M NaCl solution during 24 h, since that was the ionic strength in all experiments. The solids were separated by centrifugation and redispersed in water. These aqueous suspensions were placed on the slides and dried at 80°C.

From the contact angles of the three liquids, Young's equations like (16)

$$2\sqrt{\gamma_S^{LW}\gamma_L^{LW}} + 2\sqrt{\gamma_S^+\gamma_L^-} + 2\sqrt{\gamma_S^-\gamma_L^+} = \gamma_L(1+\cos\theta) \quad [8]$$

were written for each liquid, and the system of equations was solved in the unknowns γ_s^{LW}, γ_s^+, and γ_s^-.

Rheological Measurements

The rheological analysis of 5% (w/v) NaMt suspensions in 10^{-2} M NaCl was performed, for different pH values, in a controlled stress (Bohlin CS-25, UK) rheometer with a cup and bob (CSS 25) measuring system. Prior to each experiment, samples were presheared with a 10-Pa stress for 30 s and left to equilibrate during 180 s.

Three types of experiments were performed:

(a) Steady-state shear stress–shear rate ($\sigma - \dot{\gamma}$) measurements. All samples were subjected to a shear ramp ranging between 0.0352 and 20 Pa in 60 linearly spaced steps.

(b) Dynamic (oscillatory) measurements. The elastic, $G'(\omega)$, and viscous, $G''(\omega)$, moduli were measured for frequencies between 10^{-2} and 10^2 Hz, with a stress amplitude $\sigma_0 = 0.2$ Pa. This stress is well below the critical one, above which the viscoelastic behavior is nonlinear. The maximum deformation γ_c, attained by the system prior to getting into the nonlinear region, is related to the cohesive energy of the flocculated structure by (14, 24)

$$E_c = \frac{1}{2}G'\gamma_c^2, \quad [9]$$

where G' is the elastic modulus in the linear region.

(c) Transient (small-deformation) measurements. The viscoelastic characteristics of NaMt suspensions can also be studied in the time domain (14, 25). To that aim, a constant stress $\sigma = 0.2$ Pa is applied and the compliance, or deformation per unit stress,

$$J(t) = \frac{\gamma(t)}{\sigma} \quad [10]$$

is measured during $T = 120$ s. At $t = T$, the stress is removed, and the recovery curve is also determined.

RESULTS AND DISCUSSION

Zeta Potential

The zeta potential of NaMt particles is plotted in Fig. 1 as a function of pH (at constant ionic strength 10^{-2} M NaCl). As observed, ζ is negative for the whole pH interval, and it is essentially pH independent in good agreement with results published by other authors that suggested that edges play a negligible role

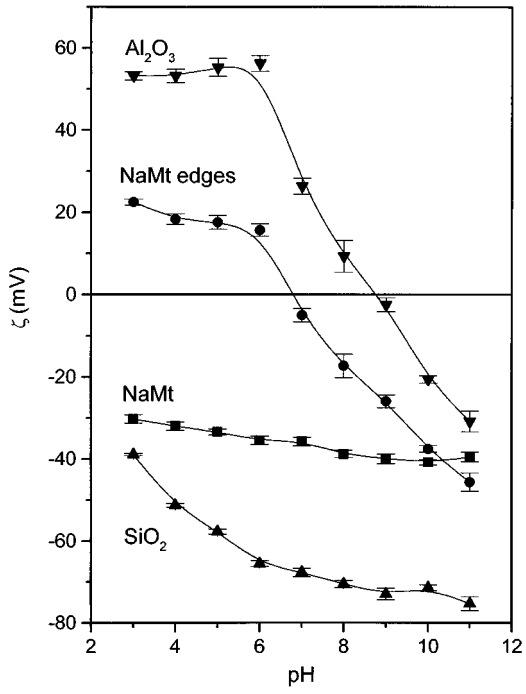

FIG. 1. Zeta potential of montmorillonite (NaMt), Al_2O_3, and SiO_2 powders as a function of pH in the presence of 10^{-2} M NaCl. The curve labeled NaMt edges was calculated as $\frac{1}{3}(\zeta_{SiO_2} + 2\zeta_{Al_2O_3})$.

in determining the electrokinetics (dominated by the constant negative charge of faces) of smectites (26–29). This fact is expected from our knowledge that only about 1% of the total surface area of montmorillonite can be ascribed to edges (28, 30).

However, edges may be essential in determining the structure of concentrated clay suspensions. That means that we need to have an estimation of the zeta potential of edges as a function of pH. Heath and Tadros (27) proposed that the isoelectric point of such surfaces must be close to that of kaolinite, i.e., $pH_{iep} \sim 7$. Other authors (9) have reported that $pH \sim 6$ is a better approximation, based on experimental data on bentonite coagulation. We adhere to the assumption made in Ref. (28); that is, the zeta potential of edges must be related to those of silica and alumina given the similarity between their surface groups. If we make the assumption that $\zeta_{edge} = \frac{1}{3}(\zeta_{SiO_2} + 2\zeta_{Al_2O_3})$, the zeta potential of edges will change with pH as shown in Fig. 1, where it can be seen that $pH_{iep} \sim 7$ for those surfaces, in agreement with Heath's and Tadros' suggestion (27).

Surface Free Energy

Using the experimental values of the contact angle θ of diiodomethane ($29.8 \pm 0.8^\circ$), water ($17 \pm 1^\circ$), and ethylene glycol ($8 \pm 1^\circ$) on NaMt, Eq. [8] allowed us to obtain γ_s^{LW}, γ_s^+, and γ_s^- for NaMt, as shown in Table 2. Based on the same assumptions as above, values calculated for the bulk sample essentially correspond to face-type surfaces and the γ components for edges could thus be calculated as a weighted mean of those of SiO_2 and Al_2O_3 ($\gamma_{edge} = 1/3(\gamma_{Silica} + 2\gamma_{Alumina})$), the latter being taken from Ref. (31). Table 2 shows that both faces and edges are almost completely monopolar and electron–donor in nature, as deduced from the fact that $\gamma_S^- \neq 0$ and $\gamma_S^+ \approx 0$.

Potential Energy of Interaction

Having obtained the zeta potentials and surface free energies of both faces and edges, the potential energies of interaction face to face (F–F), face to edge (F–E), and edge to edge (E–E) were calculated. These correspond to V_{131}, V_{132}, and V_{232}, respectively, in Fig. 2, where the relative contributions of each type of interaction (AB, LW, EL) can be distinguished. The Hamaker constants for van der Waals forces were calculated using Eq. [3] and Table 2, and the values obtained were

$$A_{131} = 7.5 \times 10^{-21}\ \text{J} \quad \text{(F–F)}$$
$$A_{132} = 7.3 \times 10^{-21}\ \text{J} \quad \text{(F–E)}$$
$$A_{232} = 6.6 \times 10^{-21}\ \text{J} \quad \text{(E–E)}.$$

The curves in Fig. 2 show some general features (repulsive short-range interaction; attractive van der Waals interaction in all cases, with a strength and range not affected by the surfaces involved), but it is most interesting to focus on the changes in EL contribution with pH. Thus, Fig. 2a (F–F) shows a repulsion that slightly increases with pH, due to the increase in $|\zeta|$ observed in Fig. 1. That trend is quite different in the case of E–F interaction (Fig. 2b): in this case, it is worth mentioning that the EL interaction is attractive at pH 5, slightly repulsive at neutral pH, and strongly repulsive at $pH > pH_{iep}$. Finally, in the edge-to-edge (E–E) interaction (Fig. 2c), the negligible electrostatic repulsion at pH 7 is the only remarkable feature.

The overall interaction is plotted in Fig. 3 for the edge-to-face interaction: whatever the pH, the curves show a rather deep attractive minimum, more important at acid pH values as a consequence of attractive electrostatic interactions between faces and edges at such pHs. Note that hydrophilic AB repulsion limits the distance of maximum approach between particles to ~10 nm. Furthermore, such distance increases slightly with pH, something that should manifest in the internal structure of the gel.

Figure 4 is intended to be a summary of the results by plotting the minimum values, V_{min}, of V_{i3j} as a function of pH. Note how face-to-face interactions are virtually independent of pH,

TABLE 2

Surface Free Energy Components of Bulk Sodium Montmorillonite (NaMt), Silica (SiO_2), Alumina (Al_2O_3), and Sodium Montmorillonite Edges (Calculated)

Material	γ^{LW} (mJ/m^2)	γ^+ (mJ/m^2)	γ^- (mJ/m^2)
NaMt	44.2 ± 0.4	0.0 ± 0.1	60.6 ± 0.5
SiO_2[a]	40.9 ± 0.1	0.1 ± 0.1	62.4 ± 0.1
Al_2O_3[a]	43.7 ± 0.1	0.0 ± 0.1	80.5 ± 0.1
NaMt (edges)	42.8 ± 0.1	0.1 ± 0.1	74.5 ± 0.1

[a] Taken from Ref. (31).

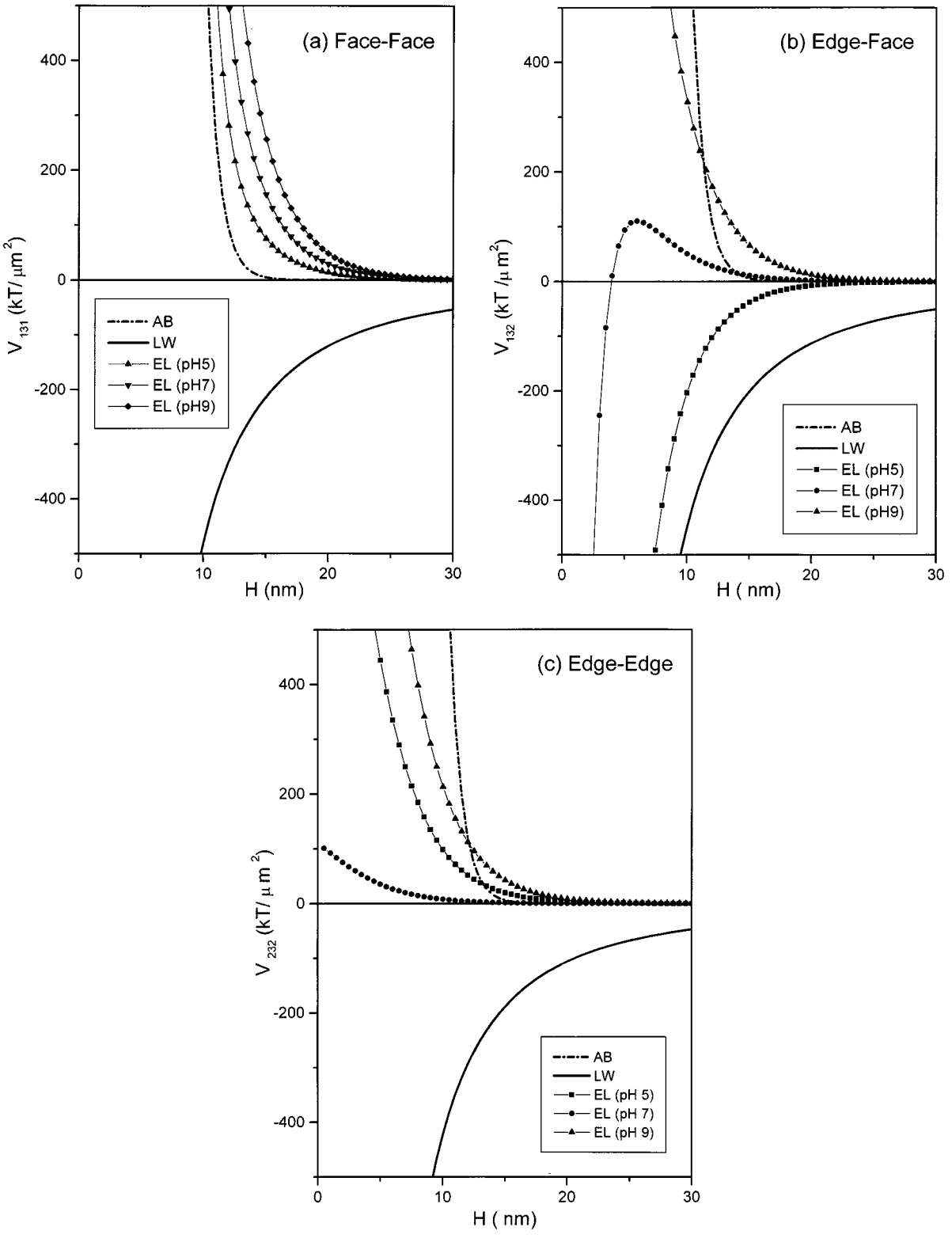

FIG. 2. Potential energy of interaction (per unit surface area) between montmorillonite particles as a function of their separation, H. Acid–base (AB), Lifshitz–van der Waals (LW), and electrostatic (EL, for different pH values) contributions. (a) Face-to-face interaction, (b) edge-to-face interaction, (c) edge-to-edge interaction.

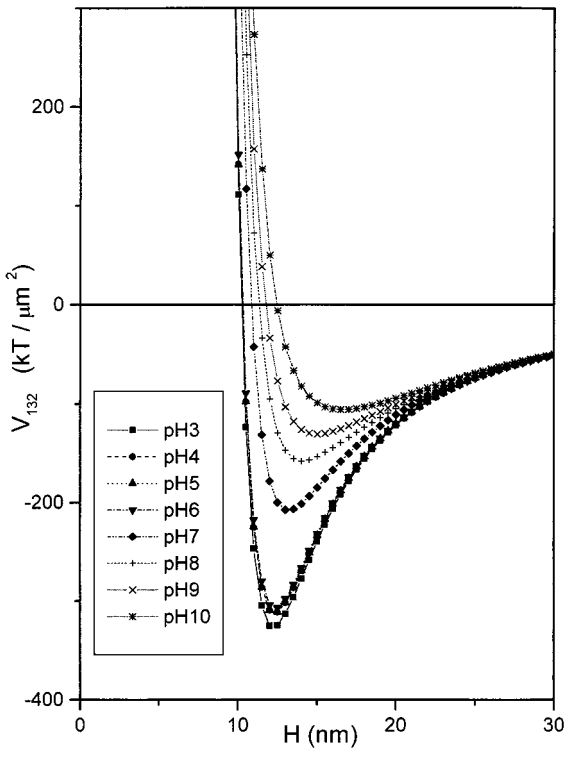

FIG. 3. Total interaction energy (per unit surface area) between edges and faces of clay particles as a function of their separation distance, for different pH values.

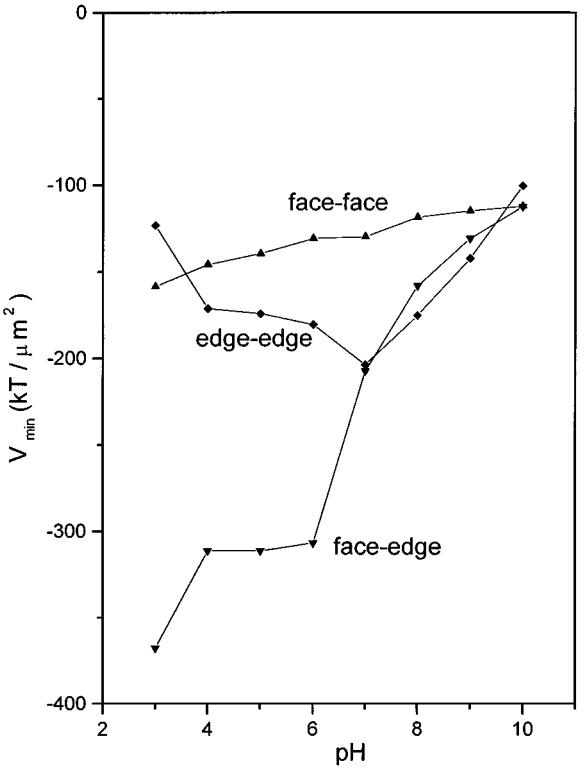

FIG. 4. Minimum value of the potential energy of interaction (F–F, E–F, and E–E) as a function of pH.

whereas edge-to-edge ones are most attractive at the iep. Undoubtedly, the most significant variations occur in edge-to-face potential energy: at basic pH it is comparable to E–E and F–F, but at pH < 7 a strong attraction is predicted that should lead to the "house-of-cards" gel structure proposed for concentrated clay suspensions in sufficiently high ionic strengths ($\geq 5 \times 10^{-3}$ M, see Refs. 26, 27, and 32).

Viscometry

Figure 5 is a log–log plot of shear stress vs shear rate data for NaMt suspensions with pH between 3 and 11. A simple visual inspection of this figure shows that, mainly for pH ≤ 7, a non-newtonian behavior of the suspensions is found: a minimum stress, σ_y, is needed for the suspensions to flow. As mentioned above, we have used two methods to estimate the yield stress: the results are depicted in Fig. 6, together with the maximum viscosity (η_{max}) of the suspensions. "σ_y (Bingham)" corresponds to the fitting of a Bingham equation ($\sigma = \sigma_y + \eta\dot{\gamma}$), and "$\sigma_y$" is the stress for which η_{max} is measured in each case. Both estimations of the yield stress change similarly with pH: σ_y decreases (up to an order of magnitude) when the pH is increased from

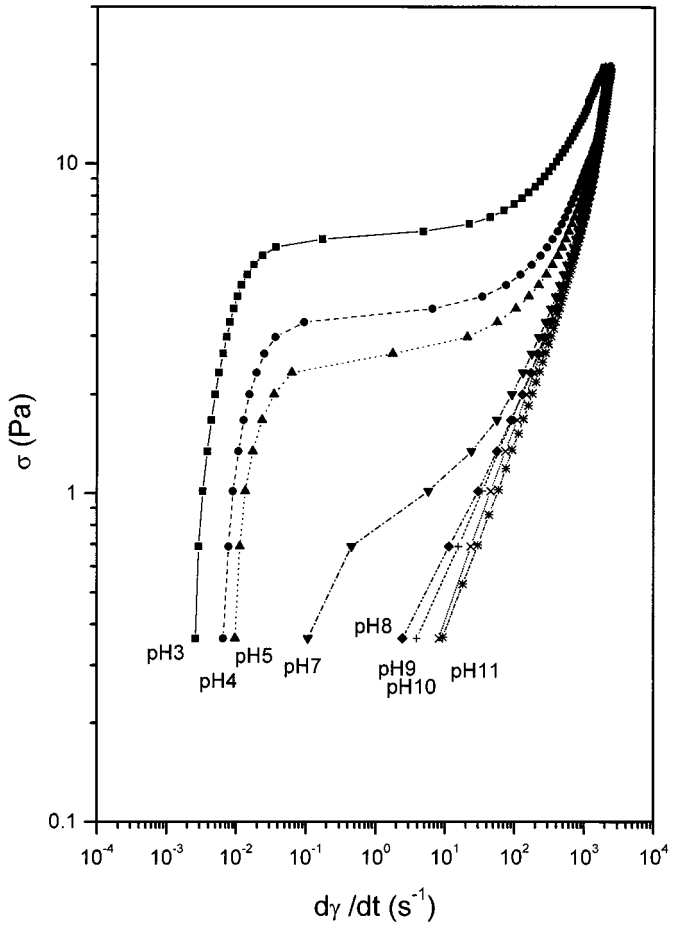

FIG. 5. Rheograms (shear stress, σ, versus shear rate, $\dot{\gamma}$) of NaMt suspensions as a function of pH.

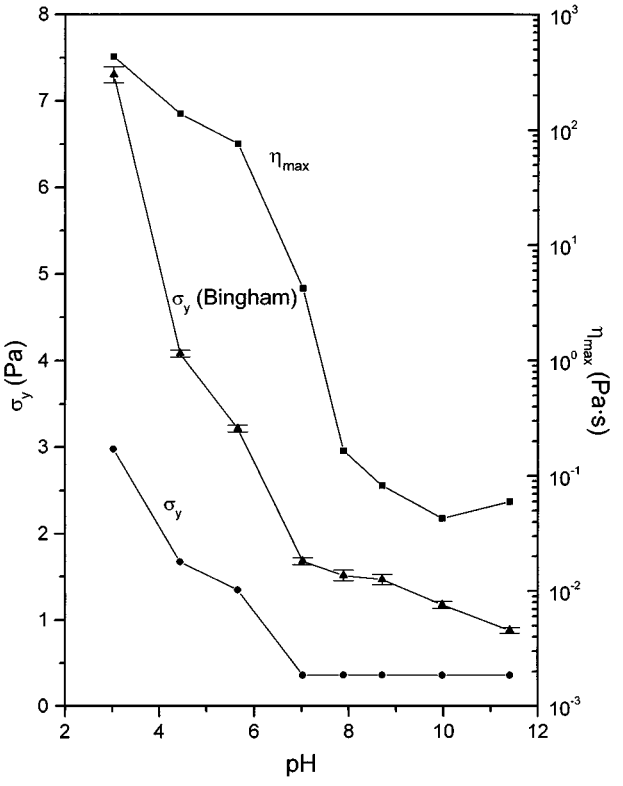

FIG. 6. Yield stress, σ_y, and maximum apparent viscosity, η_{max}, of NaMt suspensions as a function of pH. Data labeled σ_y (Bingham) were obtained by fitting the rheograms in Fig. 5 to a Bingham equation, and those labeled σ_y correspond to the maximum viscosity.

3 to 7, and a much slower decrease is found in the pH 7–11 interval. A similar trend is observed for η_{max} that diminishes in about four orders of magnitude for the whole pH range. This is in qualitative agreement with recent data by Benna *et al.* (29) on the rheology of different bentonite suspensions.

The results in Figs. 5 and 6 appear to be in qualitative agreement with our calculations of interaction energy (see, specifically, Fig. 4): the edge-to-face interaction seems to be determinant of the sharp decrease in both σ_y and η_{max} and the subsequent slow variation in the basic pH region. In the following paragraphs we try to confirm whether other rheological quantities agree with this hypothesis.

Oscillatory Measurements

Figure 7 shows the elastic modulus G' (at a frequency of 1 Hz) as a function of the amplitude of the oscillatory shear stress for different pH values. The σ_0 range for which G' is constant determines the viscoelastic linear region of the systems: it is clear that the maximum stress that the suspensions can withstand before acquiring a nonlinear viscoelasticity is lower the higher the pH. The structure can be broken more easily when the medium is basic, i.e., when all electrostatic interactions are repulsive. Furthermore, the elastic component of the complex modulus decreases by almost two orders of magnitude between pH 3 and pH 11, again confirming that the gel-like structure of the clay particles is less stiff the more basic the medium. Using Eq. [9] with the mean value of G' in the linear range, the cohesive energy density, E_c, plotted in Fig. 8 was calculated as a function of pH: as observed, there is a pronounced monotonous decrease in E_c with pH in the whole interval. All these facts can be qualitatively explained in view of the interaction energy calculations, mainly in the case of face-to-edge. Apparently, aggregates formed as a consequence of the latter attractions are determinant of the structure of the suspensions. This can be further confirmed if the relationship between G' (Fig. 7) and V_{min} (Fig. 4) is analyzed. This can be done by plotting G' (in the linear region) against V_{min} for face-to-face, face-to-edge, and edge-to-edge interactions, as shown in Fig. 9. Note that G' is a monotonously increasing function of $|V_{min}|$ in the two former cases, whereas no correlation seems to exist with V_{min} (edge-to-edge), a clear consequence of the small fraction of edge surface area as compared to that of faces.

The frequency dependencies of the elastic (G') and viscous (G'') moduli are shown in Fig. 10: both moduli are virtually independent of frequency below ~1 Hz, but, $G' > G''$, the

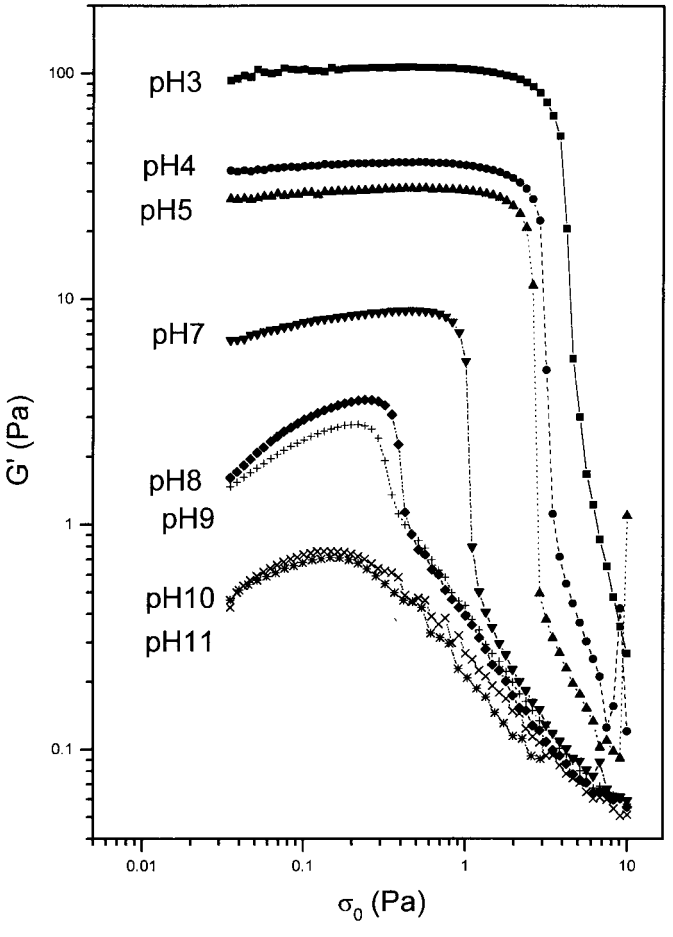

FIG. 7. Elastic modulus (real part of the complex modulus) as a function of the amplitude of the applied shear stress, for different pH values. All data were obtained for a frequency of 1 Hz.

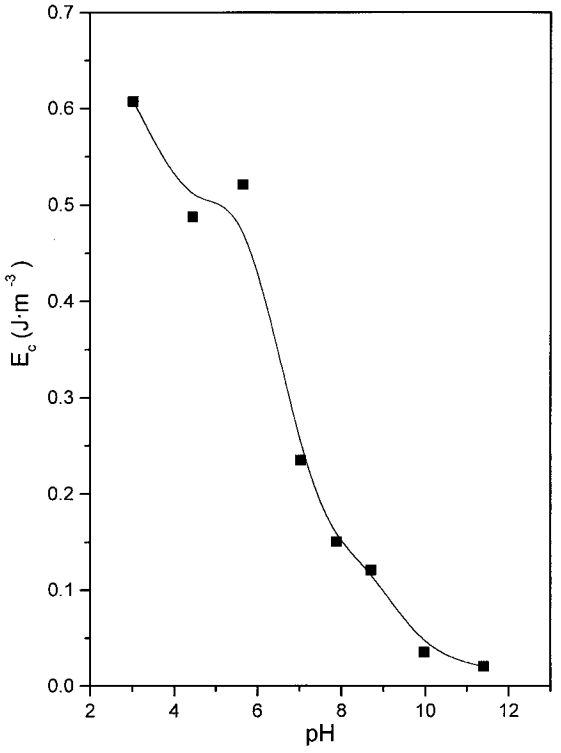

FIG. 8. Cohesive energy (per unit volume of aggregate) in NaMt suspensions, as a function of pH. Ionic strength, 10^{-2} M NaCl.

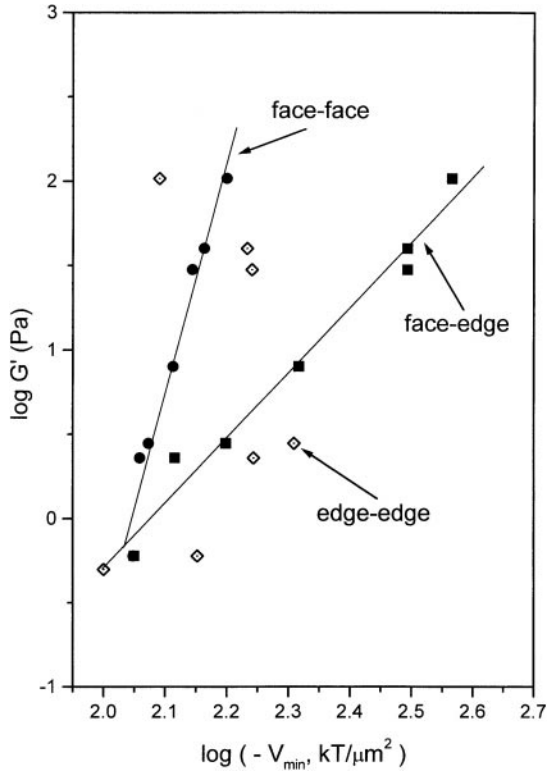

FIG. 9. Elastic modulus (average of G' in the linear region of Fig. 7) as a function of the absolute value of the minimum interaction energy face-to-face, face-to edge, and edge-to-edge.

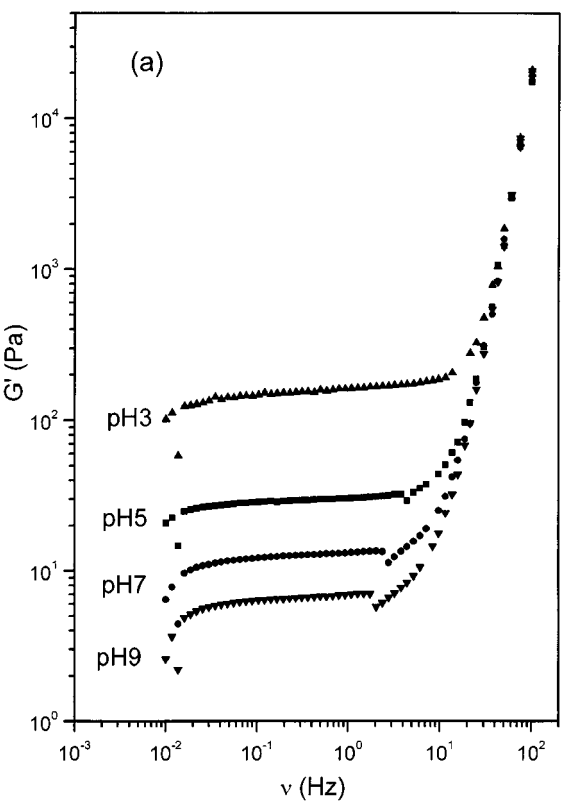

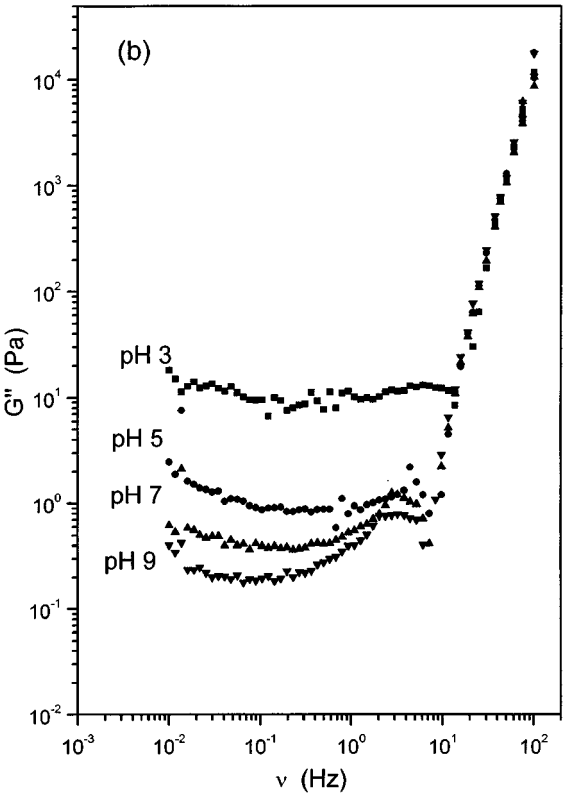

FIG. 10. Real (a) and imaginary (b) components of the complex modulus of NaMt suspensions as a function of frequency, for different pH values. Amplitude of the applied stress, 0.2 Pa.

difference being more important at acid pH values when the gel structure is expected to be stiffer. This confirms that, as stated by Tadros (14), a highly elastic, coagulated structure originated by a continuous network must characterize the suspensions in such conditions. This structure becomes more relaxed as the pH increases, in good agreement with potential energy calculations.

Creep–Recovery Data

Figure 11 shows our experimental results for the compliance function $J(t)$, defined by Eq. [10], both in creep ($t \leq 120$ s) and recovery ($t > 120$ s) conditions. In these curves the differences between the various pH values are clear: the creep deformation is much larger for basic than for acid pHs, and furthermore, the systems need longer times to reach a constant deformation during recovery. Both regions must be characteristic of systems with weak links in their internal structure, as compared to strong ones in acid solutions. This can also be easily observed if the recovery attained by the systems upon removing the stress is calculated as

$$\delta J = 100\frac{J(120) - J(240)}{J(120)} \qquad [11]$$

and plotted as a function of pH (Fig. 12). The fact that δJ is approximately 100% for pH 3 and below 50% at pH 9 indicates a behavior close to that of an elastic solid in the former conditions and more similar to a viscous fluid in the latter.

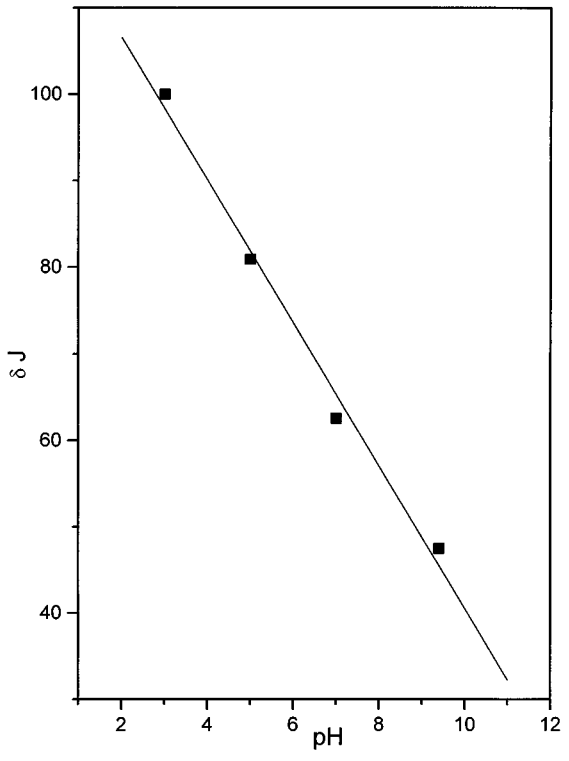

FIG. 12. Percentage recovery δJ as a function of pH. δJ was calculated from data in Fig. 11 as described in Eq. [11].

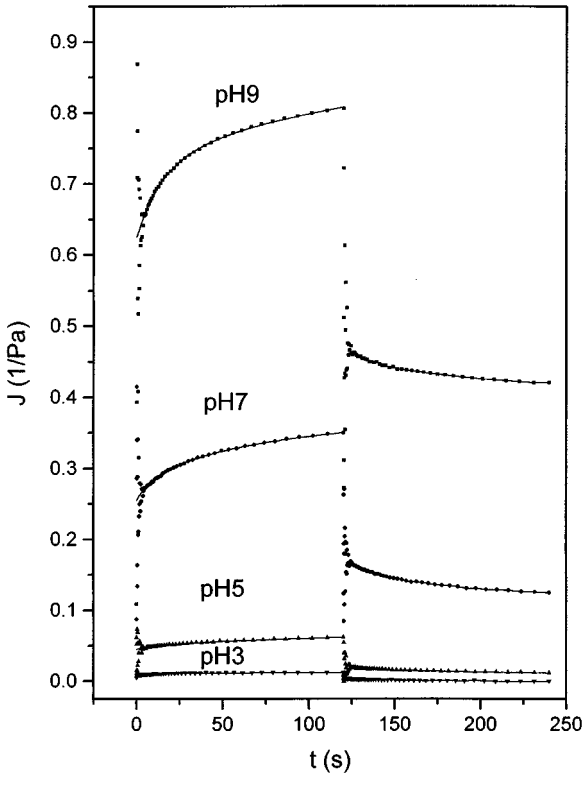

FIG. 11. Compliance function $J(t)$ as a function of time and pH. A 0.2-Pa stress step is applied at $t = 0$ and removed at $t = 120$ s.

The continuous lines drawn in Fig. 11 correspond to fitting the creep–recovery data to a Kelvin–Voigt model, a mechanical description of a viscoelastic fluid that simulates the latter as a series association of a spring of elastic constant J_0 and a viscous damper of constant η_0, together with a number of Kelvin–Voigt solids (each a parallel association of a spring J_i and a damper η_i). The creep curves are then described as (25, 33, 34)

$$J(t) = J_0 + \frac{t}{\eta_0} + \sum_i^N J_i[1 - \exp(-t/t_i)]$$

$$t_i = \frac{J_i}{\eta_i},\ i = 1, \ldots, N, \qquad [12]$$

whereas the recovery is given by

$$\gamma_r = \frac{T}{\eta_0} + \sum_i^N J_i\left(e^{T/t_i} - 1\right)e^{-t/t_i}, \qquad [13]$$

where the stress is applied for $t \leq T$ and removed at $t = T$.

The fittings in Fig. 11 were performed with just one Kelvin–Voigt solid ($N = 1$ in Eqs. [12] and [13]) and the fitting parameters are detailed in Table 3. The column J_0 represents the instantaneous unit deformation at $t = 0$; that is, the instantaneous

TABLE 3
Fitting Parameters of the Creep–Recovery Data in Fig. 12, with $N = 1$ in Eqs. [12] and [13]

	Creep				Recovery		
pH	J_0 (1/Pa)	η_0 (Pa/s)	J_1 (1/Pa)	t_1 (s)	η_0 (Pa/s)	J_1 (1/Pa)	t_1 (s)
3	0.008	—	0.004	10.1	—	0.004	37.2
5	0.045	16000	0.009	28.1	10000	0.062	48.9
7	0.230	2200	0.042	20.0	2000	0.232	225
9	0.629	2000	0.121	18.2	700	2.591	701

elastic response of the system. Note that J_0 is also the initial recovery produced at $T = 120$ s, upon ceasing the stress. The strong increase observed in J_0 when the pH is changed between 3 and 9 is the manifestation of the shift from elastic to viscous behavior in that pH range.

Concerning η_0, let us mention that it has the meaning of viscosity of the system in the newtonian ($J(t) \propto t$) regime. For pH 3, $\eta_0 \to \infty$, whereas it shows a clearly decreasing trend as the pH is increased. At low pH values, the applied stress of 0.2 Pa is not sufficient to break weak particle-to-particle bonds, and the suspensions do not flow. For higher pH values such resistance to flow is not so large, and this explains the decrease in η_0 and the increase in J_1, the so-called retarded deformation, related to the breaking and reconstruction of weak links between the particles. The characteristic relaxation time associated with these breaking/reconstruction processes is t_1. Although this time does not show a definite trend when estimated from creep data, it is clearly increasing with pH in recovery results. The system needs longer times to reach equilibrium because of the small restoring forces at high pH. Let us finally mention that η_0 and J_1 deduced from the recovery data follow the same trends (although the values are different) as those used to fit the creep curves.

CONCLUSIONS

(i) From electrophoretic mobility and contact angle measurements, we have estimated the zeta potential and surface free energy components of the different surfaces of laminar sodium montmorillonite particles. The estimations of ζ potential are based on the assumption of constant surface charge of faces and pH-dependent charge of edges. In particular, it is assumed that surface properties of edges can be considered as a weighted average of that of silica and alumina, this yielding an isoelectric point of edges at pH ~ 7. With these assumptions it appeared possible to justify the experimental rheological behavior of concentrated clay suspensions at variable pH and constant ionic strength (10^{-2} M).

(ii) From the precedent estimation of surface properties of faces and edges, it is possible to calculate the total F–F, E–E, and F–E energy of interaction (extended DLVO theory). It was found that face-to-edge attraction is the predominant interaction in the acid pH range and determines the internal structure of the gel in these conditions. At basic pH, the attraction between different surfaces is weaker and a more relaxed internal structure of the system is predicted.

(iii) Steady-state rheological measurements show a sharp decrease in the yield stress of the suspensions from acid to basic pH, in good agreement with the predictions of face–edge attraction energy. Oscillatory measurements demonstrate that the behavior of the suspensions is more elastic than viscous (storage modulus larger than loss modulus), mainly in the acid pH range. The cohesive energy of the flocs decreases by more than one order of magnitude from pH 3 to pH 11, in agreement with the sharp decrease of face–edge attraction in this pH range. Transient measurements (creep–recovery experiments) confirm the predominant role played by this type of interaction in the configuration of the internal structure of NaMt concentrated suspensions.

ACKNOWLEDGMENTS

Financial support by CICYT, Spain (Project No. MAT98-0940), and INTAS (Project No. INTAS/UA-95/0165) is gratefully acknowledged.

REFERENCES

1. Tadros, Th. F., *Rev. Inst. Fr. Pét.* **52,** 199 (1997).
2. Craig, D. Q. M., Tamburic, S., Buckton, G., and Newton, J. M., *J. Control. Release* **30,** 213 (1994).
3. Cabrerizo, M. A., Gallardo, V., Ruiz, M. A., and Parera, A., *Cosmet. Toiletries* **104,** 49 (1989).
4. Linares, J., *Enresa Tech. Publ. No. 1* (1993). [In Spanish]
5. Cancela, G., Taboada, E. R., and Sánchez-Rasero, F., *J. Soil Sci.* **43,** 99 (1992).
6. Bereket, G., Aroguz, A. Z., and Özel, M. Z., *J. Colloid Interface Sci.* **187,** 338 (1997).
7. Altin, O., Ölbelge, H. O., and Dogu, T., *J. Colloid Interface Sci.* **198,** 130 (1998).
8. Sondi, I., and Pravdić, *V. Croat. Chem. Acta* **71,** 1061 (1998).
9. Permien, T., and Lagaly, G., *Clay Miner.* **29,** 751, (1994); **29,** 761 (1994).
10. Permien, T., and Lagaly, G., *Clays Clay Miner.* **43,** 229 (1995).
11. Buscall, R., Goodwin, J. W., and Ottewill, R. H., *J. Chem. Soc. Faraday Trans. 1* **78,** 2889 (1982).
12. Tadros, Th. F., *Langmuir* **6,** 28 (1990).
13. Tadros, Th. F., Liang, W., Costello, B., and Luckham, P. F., *Colloids Surf. A* **79,** 105 (1993).
14. Tadros, Th. F., *Adv. Colloid Interface Sci.* **68,** 97 (1996).
15. Israelechvili, J., "Intermolecular and Surface Forces." Academic Press. London 1991.
16. Van Oss, C. J., "Interfacial Forces in Aqueous Media." Dekker, New York/Hong Kong, 1994.
17. Arroyo, F. J., Carrique, F., Jiménez-Olivares, M. L., and Delgado, A. V., *J. Colloid Interface Sci.* **229,** 118 (2000).
18. Hogg, R., Healy, T. W., and Fuerstenau, D. W., *Trans. Faraday Soc.* **62,** 1638 (1966).
19. Usui, S., *in* "Electrical Phenomena at Interfaces" (H. Oshima and K. Furusawa, Eds.), p. 101. Dekker, New York, 1998.
20. Van Oss, C. J., Chaudhury, M. K., and Good, R. J., *Chem. Rev.* **88,** 972 (1988).
21. Van Olphen, H., "An Introduction to Clay Colloid Chemistry." Wiley Interscience, New York, 1977.
22. Altin, A., Özbelge, H. O., and Dogn, T., *J. Colloid Interface Sci.* **217,** 19 (1999).

23. Adamson, A. W., "Physical Chemistry of Surfaces." Wiley Interscience, New York, 1967.
24. Ramsay, J. D. G., Daish, S. R., and Wright, G. J., *Faraday Discuss Chem. Soc.* **65,** 65 (1978).
25. Deem, D. E., *in* "Pharmaceutical Dosage Forms: Disperse Systems" (H. A. Lieberman, M. M. Rieger, and G. S. Bauker, Eds.), Vol. I, Chap. 9 Dekker, New York, 1988.
26. Callaghan, I. C., and Ottewill, R. H., *Faraday Discuss. Chem. Soc.* **57,** 110 (1974).
27. Heath, O., and Tadros, Th. F., *J. Colloid Interface Sci.* **93,** 307 (1983).
28. Sondi, I., Milat, O., and Pravdic, V., *J. Colloid Interface Sci.* **189,** 66 (1997).
29. Benna, M., K-bir-Ariguib, N., Magnin, A., and Bergaga, F., *J. Colloid Interface Sci.* **218,** 442 (1999).
30. Dyal, R. S., and Hendricks, S. B., *Soil Sci.* **69,** 421 (1950).
31. Chibowski, E., *in* "Contact Angle, Wettability and Adhesion" (K. L. Mittal, Ed.), p. 641. U.S.P., Utrecht, 1993.
32. Ravid, B., Pekenc, E., Goodwin, J. W., and Smith, R. W., *J. Chem. Soc. Faraday Trans.* **76,** 225 (1980).
33. Courraze, G., and Grossiord, J. L., "Initiation à la Rheologie," Chap. II. Lavoisier, Paris, 1983.
34. Tadros, Th. F., *in* "Solid/Liquid Dispersions" (Th. F. Tadros, Ed.), p. 293. Academic Press, London, 1987.